

## Experimental study on the behaviour of the submerged jet in a cold liquid metal model for continuous casting of round blooms under the influence of rotating magnetic fields

D. Schurmann, B. Willers, S. Eckert

Helmholtz-Zentrum Dresden-Rossendorf e.V. (HZDR), Bautzner Landstraße 400, 01328  
Dresden, Germany

Corresponding author: d.schurmann@hzdr.de

### Abstract

Experimental results were obtained at the Mini-LIMMCAST facility [1], an experimental setup to model continuous casting of steel operated continuously as a loop with the cold liquid metal alloy GaInSn. The setup consists of a round mould with an inner diameter of 80 mm, representing a mould used in industrial bloom casting in a scale of 1:3. A mould-electromagnetic-stirrer (M-EMS) generated a rotating magnetic field (RMF) with different magnetic flux densities. Velocity profiles inside the mould were measured by Ultrasound Doppler Velocimetry (UDV). The experiments revealed an unexpected behaviour of the submerged jet: for medium magnetic field strengths of the RMF it can be observed, that the jet stops circling and stays at one position in the mould, bearing the risk of breakout due to continuous impingement of superheated material to one position of the solidified shell.

**Key words:** Liquid Metal Model, Ultrasound Doppler Velocimetry (UDV), Continuous Casting, Rotating Magnetic Field (RMF)

### Introduction

In the continuous casting process of round blooms or billets Rotating Magnetic Fields (RMF) applied by electromagnetic-stirrers (EMS) are widely used to promote equiaxed solidification and therefore an improved quality of the cast product. In a recent study [2] we showed that intensive stirring results in high horizontal velocities in the vicinity of the meniscus and creates swirl structures at the free surface which might be responsible for bringing inclusions from the slag layer into the solidification zone. In this study we investigate the vertical velocities that develop in the mould caused by the jet which emerges from the submerged entry nozzle (SEN) under the influence of different strengths of the rotating magnetic field.

### Experimental Setup

The LIMMCAST experimental facilities at HZDR are used to model the continuous casting process in low temperature liquid metal experiments [1, 3]. The facilities allow investigations of several aspects of the continuous casting process and focus mainly on the determination of the flow structures that develop in the continuous casting mould. The high versatility of the facilities allow measurements in different casting geometries, also under the influence of magnetic fields.

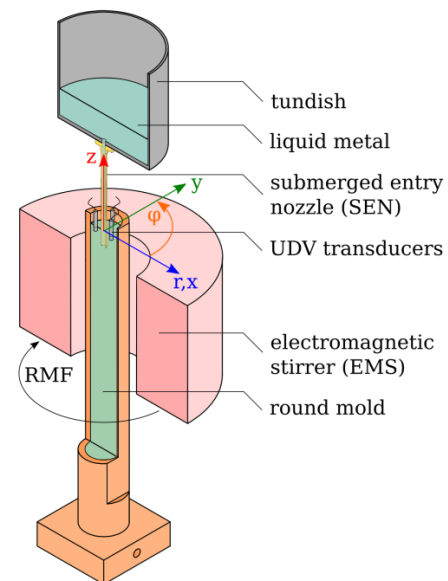


Fig. 1: Schematic view of the setup.

Table 1: Some physical properties of liquid steel at 1500 °C and GaInSn and water at 20 °C. The values for liquid steel are exemplary values from [4], [5], GaInSn values are from measurements [6] and water from [7].

		Liquid Steel	GaInSn	Water
density	kg / m <sup>3</sup>	~ 7 000	6 353	988
dyn. viscosity	mPa s	~ 2 ... 18	2.1	1
el. conductivity	1 / Ω m	~ 0.833 × 10 <sup>6</sup>	3.29 × 10 <sup>6</sup>	<50



The study presented in this work is performed at the Mini-LIMMCAST facility, which is composed of a liquid metal loop, operated at room temperature with GaInSn. Some physical properties of the model fluid are compared to those of liquid steel and water in Table 1. From the low electrical conductivity of water compared to that of steel it can be concluded that the use of a liquid metal as a model fluid is compulsory when the influence of magnetic fields are of interest.

Fig. 1 shows a schematic view of the setup. The liquid metal is pumped continuously from a storage vessel into the tundish, where the level is kept constant, by controlling the rotation speed of the pump. Driven by gravity, the liquid metal flows through the SEN into the model of mould and strand, over a dam to set a constant level of the meniscus inside the mould and finally back into the storage vessel. The PMMA model of mould and strand represent an industrial configuration in a scale of 1:3 for continuous casting of round blooms. It has an inner diameter of 80 mm and a length of approx. 800 mm. The submerged entry nozzle (SEN) has a single vertical outlet with a diameter of 10 mm. A mould electromagnetic stirrer, positioned between  $-380 \text{ mm} < z < -70 \text{ mm}$ , is used to apply a rotating magnetic field (RMF) with a frequency of  $f = 2.5 \text{ Hz}$  and a magnetic flux density of up to  $B_0 = 20 \text{ mT}$  to the set up. The coordinate system for the measurements is located in the centre of the cylindrical model with the  $z$ -axis pointing to the top and  $z = 0$  located on the free surface in the model mould.

Measurements of the vertical velocity component  $w$  are performed by means of Ultrasound Doppler Velocimetry (UDV) by a DOP 3010 (Signal Processing S.A., Savigny, Switzerland, [8]) with up to ten individual ultrasound transducers. The transducers are positioned at  $z = -10 \text{ mm}$  in direct contact with the liquid metal, every  $90^\circ$  at radial positions of  $r = 30 \text{ mm}$ .

### Results

A tempo-spatial contour plot of a three minute long measurement of the vertical velocity component  $w$  from below the meniscus down to  $z = -300 \text{ mm}$  in the mould at four sensor locations on the radius  $r = 30 \text{ mm}$  is shown in Fig. 2. The magnetic flux density  $B_0$  of the RMF has been increased two times, at  $t = 62 \text{ s}$  from  $B_0 = 10 \text{ mT}$  to  $15 \text{ mT}$ , and finally at  $t = 125 \text{ s}$  to  $B_0 = 20 \text{ mT}$ .

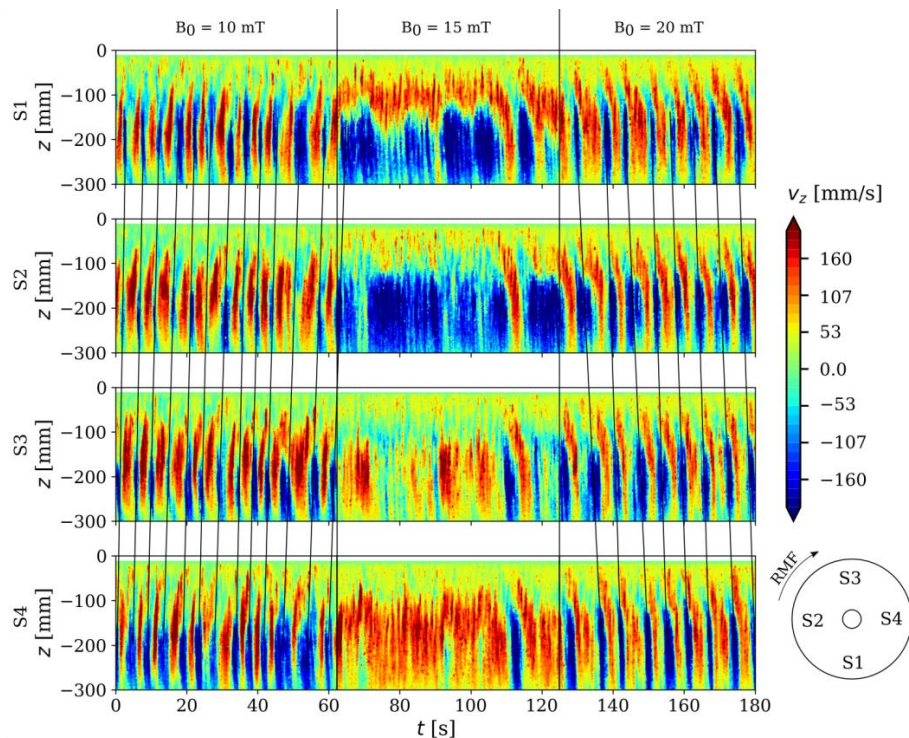


Fig. 2: Time evolution of the vertical velocity component measured by four sensors in the mould at  $r = 30 \text{ mm}$  under the influence of three different magnetic flux densities  $B_0$ .

In the first part of the measurement, where a small magnetic flux density of  $B_0 = 10$  mT is applied ( $t < 62$  s), a periodic oscillation between positive and negative velocities can be observed at each sensor. A negative velocity is detected when the submerged jet, which emerges from the SEN, passes the measurement line of the ultrasound transducer. A positive velocity represents an upward flow to the free surface. The velocities are shifted in time between the sensors, which indicates a circling movement from one sensor to the other. The tilted black lines in the diagram show that the jet passes the sensors in a counter-clockwise direction, which is opposite to the rotating direction of the RMF as applied here to the setup.

At a medium magnetic flux density of 15 mT ( $62 \text{ s} < t < 125 \text{ s}$ ) the periodic oscillation between upward and downward flow cannot be observed any more. Negative velocities which represent the presence of the jet are primarily measured by sensor S1 and S2, while the upward flow is recorded by the sensors at the opposite site of the mould. This means that the jet stops its circling motion through the mould and stays mainly at one position. The magnetic flux density at which the circling of the jet stops is referred to as critical magnetic flux density  $B_{0,crit}$ .

At higher magnetic flux densities of the RMF ( $B_0 = 20$  mT,  $t > 125$  s) a behaviour similar to the lowest RMF can be observed: a periodic change of positive and negative velocities at each sensor and a time-shift from sensor to sensor, indicating the circling of the jet inside the mould. In contrast to the first part, at  $B_0 = 20$  mT the circling direction of the jet is clockwise, which is in the same direction in which the RMF is applied.

To quantify the circling behaviour of the jet, measurements of the vertical velocity component  $w$  in the mould with six different magnetic flux densities from  $B_0 = 2.4$  mT to 19.8 mT are performed. A discrete fast-Fourier-transformation (FFT) is applied to the velocity data which is measured along the three dimensions time  $t$ , angular position of the UDV transducers  $\varphi$  and measurement depth  $z$  at discrete values ( $k, l, m$ ):

$$w = w_{klm}(z_k, \varphi_l, t_m) \quad k = 1 \dots K, \quad l = 1 \dots L, \quad m = 1 \dots M \quad (1)$$

The 3d-FFT is then defined as

$$W_{\chi\psi f} = \sum_{k=1}^K \sum_{l=1}^L \sum_{m=1}^M w_{klm} e^{-j2\pi(\chi k/K + \psi l/L + f m/M)} \quad (2)$$

and yields the three frequencies  $\chi, \psi, f$ , which are related to the three dimensions  $z, \varphi, t$  of the measurement. Extracting the frequency  $f$ , where the absolute value of the FFT is maximal, allows the quantification of the jet's circling frequency and direction.

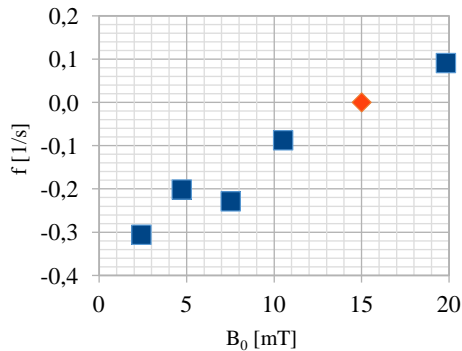


Fig. 3: Circling frequencies  $f$  of the jet for different magnetic flux densities  $B_0$  of the RMF.

The extracted frequencies for the measurements with variable  $B_0$  are shown in Fig. 3. Three situations can be distinguished: for magnetic flux densities which are smaller than the critical value  $B_{0,crit}$ , negative circling frequencies can be observed, which corresponds to a circling of the jet in opposite direction than the applied RMF. The closer  $B_0$  is to the critical magnetic flux density, the lower the circling frequency of the jet. As mentioned earlier, at the critical value  $B_{0,crit} = 15$  mT no significant circling of the jet can be observed, which corresponds to a circling frequency of  $f = 0$ . For increasing magnetic flux densities a positive circling frequency, corresponding to a circling of the jet in the same direction as the applied RMF is found. Frequencies between  $-0.3 \text{ Hz} \leq f \leq 0.1 \text{ Hz}$  were found.

## Discussion

By measuring the tangential velocity in this configuration it was shown in [2], that with increasing magnetic flux density of the RMF the rotation of the fluid in the strand intensifies.

When we assume that the jet is disturbed and enters the rotating fluid column a bit off centre, it will be deformed in the direction of the main rotational flow. The fluid that leaves the jet is responsible for a momentum transport and therefore

a propelling of the jet. If the kinetic energy of the deformed jet is higher than that of the rotating column, the jet is able to propel itself against the direction of the cylindrical flow. This is the case for a low RMF or a high casting speed. When the magnetic flux density of the RMF is increased towards  $B_{0,crit}$ , the kinetic energies of jet and rotating fluid column are similar and the momentum transport of the deformed jet is not high enough to propel the jet against the fluid column, resulting in a stop of the jet circling. If the RMF is above the critical magnetic flux density, the jet's momentum transport is not sufficient to propel itself against the rotating fluid column, but gets slowly transported in the direction of the rotating fluid column. Therefore, the frequencies which could be extracted from the FFT in Fig. 3 are below those of the rotating fluid column (c.f. [2]) and much lower than the frequency of the applied RMF.

The situation when the jet stops circling at  $B_0 = B_{0,crit}$  can be dangerous for the real process, since the superheated material brought to one side of the mould by the jet would remelt and weaken the solidified strand shell. Therefore, the shell might not be able to withstand the high pressure of the liquid steel in the mould and break, causing an expensive stop of the production. Therefore we suggest to avoid the operation of a continuous casting strand with the application of a RMF close to the critical magnetic flux density of the particular system. It is very likely, that this critical parameter is dependent on the casting velocity and the geometric parameters of mould and SEN. With a higher casting velocity the kinetic energy of the jet increases, which would move the critical magnetic flux density to higher values. In contrast, a lower casting speed and therefore a lower kinetic energy of the jet will probably move the critical magnetic flux density to lower values. Therefore, when a reduction of the casting velocity occurs, e.g. at the end of the casting process, when less liquid steel is in the tundish, the magnetic flux density of the RMF has to be adapted accordingly, to avoid the critical value for that casting speed.

### Conclusions

Measurements of the vertical velocities in a cold liquid metal model for the continuous casting of round blooms with applied electromagnetic stirring have been performed at the Mini-LIMMCAST facility of HZDR by means of the Ultrasound Doppler Velocimetry.

The measurements revealed several interesting phenomena related to the behaviour of the submerged jet under the influence of rotating magnetic fields, which have not been described before:

1. The jet circles in the mould.
2. The jet stops circling at a critical magnetic flux density  $B_{0,crit}$ , which should be avoided in the casting process to prevent a possible breakout of liquid steel out of the strand.
3. The jet circulation direction depends on the magnetic flux density of the RMF:
  - a.  $B_0 < B_{0,crit}$ : The jet circles in opposite direction than the RMF.
  - b.  $B_0 > B_{0,crit}$ : The jet circles in the same direction as the RMF.
4. The circling frequency of the jet is much lower than the rotational frequency of the RMF.

### References

1. K. Timmel, S. Eckert, G. Gerbeth, F. Stefani, and T. Wondrak, 'Experimental Modeling of the Continuous Casting Process of Steel Using Low Melting Point Metal Alloys - the LIMMCAST Program', *ISIJ Int.*, vol. 50, no. 8, pp. 1134–1141, 2010.
2. B. Willers, M. Barna, J. Reiter, and S. Eckert, 'Experimental Investigations of Rotary Electromagnetic Mould Stirring in Continuous Casting Using a Cold Liquid Metal Model', *ISIJ Int.*, vol. 57, no. 3, pp. 468–477, 2017.
3. K. Timmel, C. Kratzsch, A. Asad, D. Schurmann, R. Schwarze, and S. Eckert, 'Experimental and Numerical Modeling of Fluid Flow Processes in Continuous Casting: Results from the LIMMCAST-Project', *IOP Conf. Ser. Mater. Sci. Eng.*, vol. 228, p. 012019, Jul. 2017.
4. C. Y. Ho and T. K. Chu, 'Electrical resistivity and thermal conductivity of nine selected AISI stainless steels', DTIC Document, 1977.
5. M. Korolczuk-Hejnak, P. Migas, and W. Ślęzak, 'Determination of the liquid steel viscosity curves using a high temperature rheometer', *J. Phys. Conf. Ser.*, vol. 602, p. 012037, Apr. 2015.
6. Y. Plevachuk, V. Sklyarchuk, S. Eckert, G. Gerbeth, and R. Novakovic, 'Thermophysical Properties of the Liquid Ga-In-Sn Eutectic Alloy', *J. Chem. Eng. Data*, vol. 59, no. 3, pp. 757–763, Mar. 2014.
7. VDI, Ed., *VDI-Wärmeatlas*, 11th ed. Berlin, Heidelberg: Springer, 2013.
8. S. A. Signal Processing, 'DOP3000 series User's manual'.